Multi-wavelength Observations of the Flaring Gamma-ray Blazar 3C 66A in 2008 October

A. A. Abdo[1,2], M. Ackermann[3], M. Ajello[3], L. Baldini[4], J. Ballet[5], G. Barbiellini[6,7], D. Bastieri[8,9], K. Bechtol[3], R. Bellazzini[4], B. Berenji[3], R. D. Blandford[3], E. Bonamente[10,11], A. W. Borgland[3], A. Bouvier[3], J. Bregeon[4], A. Brez[4], M. Brigida[12,13], P. Bruel[14], R. Buehler[3], S. Buson[8,9], G. A. Caliandro[15], R. A. Cameron[3], P. A. Caraveo[16], S. Carrigan[9], J. M. Casandjian[5], E. Cavazzuti[17], C. Cecchi[10,11], Ö. Çelik[18,19,20], E. Charles[3], A. Chekhtman[1,21], C. C. Cheung[1,2], J. Chiang[3], S. Ciprini[11], R. Claus[3], J. Cohen-Tanugi[22], J. Conrad[23,24,25], L. Costamante[3], S. Cutini[17], D. S. Davis[18,20], C. D. Dermer[1], F. de Palma[12,13], S. W. Digel[3], E. do Couto e Silva[3], P. S. Drell[3], R. Dubois[3], D. Dumora[26,27], C. Favuzzi[12,13], S. J. Fegan[14], P. Fortin[14], M. Frailis[28,29], L. Fuhrmann[30], Y. Fukazawa[31], S. Funk[3], P. Fusco[12,13], F. Gargano[13], D. Gasparrini[17], N. Gehrels[18], S. Germani[10,11], N. Giglietto[12,13], P. Giommi[17], F. Giordano[12,13], M. Giroletti[32], T. Glanzman[3], G. Godfrey[3], I. A. Grenier[5], J. E. Grove[1], L. Guillemot[30,26,27], S. Guiriec[33], D. Hadasch[15], M. Hayashida[3], E. Hays[18], D. Horan[14], R. E. Hughes[34], R. Itoh[31], G. Jóhannesson[3], A. S. Johnson[3], T. J. Johnson[18,35], W. N. Johnson[1], T. Kamae[3], H. Katagiri[31], J. Kataoka[36], J. Knödlseder[37], M. Kuss[4], J. Lande[3], L. Latronico[4], S.-H. Lee[3], F. Longo[6,7], F. Loparco[12,13], B. Lott[26,27], M. N. Lovellette[1], P. Lubrano[10,11], A. Makeev[1,21], M. N. Mazziotta[13], J. E. McEnery[18,35], J. Mehault[22], P. F. Michelson[3], T. Mizuno[31], A. A. Moiseev[19,35], C. Monte[12,13], M. E. Monzani[3], A. Morselli[38], I. V. Moskalenko[3], S. Murgia[3], T. Nakamori[36], M. Naumann-Godo[5], I. Nestoras[30], P. L. Nolan[3], J. P. Norris[39], E. Nuss[22], T. Ohsugi[40], A. Okumura[41], N. Omodei[3], E. Orlando[42], J. F. Ormes[39], M. Ozaki[41], D. Paneque[3], J. H. Panetta[3], D. Parent[1,21], V. Pelassa[22], M. Pepe[10,11], M. Pesce-Rollins[4], F. Piron[22], T. A. Porter[3], S. Rainò[12,13], R. Rando[8,9], M. Razzano[4], A. Reimer[43,3], O. Reimer[43,3], L. C. Reyes[44], J. Ripken[23,24], S. Ritz[45], R. W. Romani[3], M. Roth[46], H. F.-W. Sadrozinski[45], D. Sanchez[14], A. Sander[34], J. D. Scargle[47], C. Sgrò[4], M. S. Shaw[3], P. D. Smith[34], G. Spandre[4], P. Spinelli[12,13], M. S. Strickman[1], D. J. Suson[48], H. Takahashi[40], T. Tanaka[3], J. B. Thayer[3], J. G. Thayer[3], D. J. Thompson[18], L. Tibaldo[8,9,5,49], D. F. Torres[15,50], G. Tosti[10,11], A. Tramacere[3,51,52], T. L. Usher[3], J. Vandenbroucke[3], V. Vasileiou[19,20], N. Vilchez[37], V. Vitale[38,53], A. P. Waite[3], P. Wang[3], B. L. Winer[34], K. S. Wood[1], Z. Yang[23,24], T. Ylinen[54,55,24], M. Ziegler[45] (The Fermi-LAT Collaboration), V. A. Acciari[56], E. Aliu[57], T. Arlen[58], T. Aune[59], M. Beilicke[60], W. Benbow[56], M. Böttcher[61], D. Boltuch[62], S. M. Bradbury[63], J. H. Buckley[60], V. Bugaev[60], K. Byrum[64], A. Cannon[65], A. Cesarini[66], J. L. Christiansen[67], L. Ciupik[68], W. Cui[69], I. de la Calle Perez[70], R. Dickherber[60], M. Errando[57], A. Falcone[71], J. P. Finley[69], G. Finnegan[72], L. Fortson[68], A. Furniss[59], N. Galante[56], D. Gall[69], G. H. Gillanders[66], S. Godambe[72], J. Grube[68], R. Guenette[73], G. Gyuk[68], D. Hanna[73], J. Holder[62], C. M. Hui[72], T. B. Humensky[74], A. Imran[75], P. Kaaret[76], N. Karlsson[68], M. Kertzman[77], D. Kieda[72], A. Konopelko[78], H. Krawczynski[60], F. Krennrich[75], M. J. Lang[66], S. LeBohec[72], G. Maier[73,120], S. McArthur[60], A. McCann[73], M. McCutcheon[73], P. Moriarty[79], R. Mukherjee[57], R. A. Ong[58], A. N. Otte[59], D. Pandel[76], J. S. Perkins[56], A. Pichel[80], M. Pohl[75,121], J. Quinn[65], K. Ragan[73], P. T. Reynolds[81], E. Roache[56], H. J. Rose[63],

M. Schroedter[75], G. H. Sembroski[69], G. Demet Senturk[82], A. W. Smith[64], D. Steele[68,123],
S. P. Swordy[74], G. Tešić[73], M. Theiling[56], S. Thibadeau[60], A. Varlotta[69], V. V. Vassiliev[58],
S. Vincent[72], S. P. Wakely[74], J. E. Ward[65], T. C. Weekes[56], A. Weinstein[58], T. Weisgarber[74],
D. A. Williams[59], S. Wissel[74], M. Wood[58] (the VERITAS Collaboration),
M. Villata[83], C. M. Raiteri[83], M. A. Gurwell[84], V. M. Larionov[85,86,87], O. M. Kurtanidze[88],
M. F. Aller[89], A. Lähteenmäki[90], W. P. Chen[91], A. Berduygin[92], I. Agudo[93], H. D. Aller[89],
A. A. Arkharov[86], U. Bach[94], R. Bachev[95], P. Beltrame[96], E. Benítez[97], C. S. Buemi[98],
J. Dashti[99], P. Calcidese[100], D. Capezzali[101], D. Carosati[101], D. Da Rio[96], A. Di Paola[102],
C. Diltz[99], M. Dolci[103], D. Dultzin[97], E. Forné[104], J. L. Gómez[93], V. A. Hagen-Thorn[85,87],
A. Halkola[92], J. Heidt[105], D. Hiriart[106], T. Hovatta[90], H.-Y. Hsiao[91], S. G. Jorstad[107],
G. N. Kimeridze[88], T. S. Konstantinova[85], E. N. Kopatskaya[85], E. Koptelova[91], P. Leto[98],
R. Ligustri[96], E. Lindfors[92], J. M. Lopez[106], A. P. Marscher[107], M. Mommert[105,108], R. Mujica[109],
M. G. Nikolashvili[88], K. Nilsson[110], N. Palma[99], M. Pasanen[92], M. Roca-Sogorb[93], J. A. Ros[104],
P. Roustazadeh[99], A. C. Sadun[111], J. Saino[92], L. A. Sigua[88], A. Sillanää[92], M. Sorcia[97],
L. O. Takalo[92], M. Tornikoski[90], C. Trigilio[98], R. Turchetti[96], G. Umana[98]
(the GASP-WEBT Consortium),
T. Belloni[112] C. H. Blake[113], J. S. Bloom[114], E. Angelakis[115], M. Fumagalli[116] M. Hauser[117],
J. X. Prochaska[116,118], D. Riquelme[119], A. Sievers[119], D. L. Starr[114], G. Tagliaferri[112]
H. Ungerechts[119], S. Wagner[117], J. A. Zensus[115]

[1]Space Science Division, Naval Research Laboratory, Washington, DC 20375, USA

[2]National Research Council Research Associate, National Academy of Sciences, Washington, DC 20001, USA

[3]W. W. Hansen Experimental Physics Laboratory, Kavli Institute for Particle Astrophysics and Cosmology, Department of Physics and SLAC National Accelerator Laboratory, Stanford University, Stanford, CA 94305, USA

[4]Istituto Nazionale di Fisica Nucleare, Sezione di Pisa, I-56127 Pisa, Italy

[5]Laboratoire AIM, CEA-IRFU/CNRS/Université Paris Diderot, Service d'Astrophysique, CEA Saclay, 91191 Gif sur Yvette, France

[6]Istituto Nazionale di Fisica Nucleare, Sezione di Trieste, I-34127 Trieste, Italy

[7]Dipartimento di Fisica, Università di Trieste, I-34127 Trieste, Italy

[8]Istituto Nazionale di Fisica Nucleare, Sezione di Padova, I-35131 Padova, Italy

[9]Dipartimento di Fisica "G. Galilei", Università di Padova, I-35131 Padova, Italy

[10]Istituto Nazionale di Fisica Nucleare, Sezione di Perugia, I-06123 Perugia, Italy

[11]Dipartimento di Fisica, Università degli Studi di Perugia, I-06123 Perugia, Italy

[12]Dipartimento di Fisica "M. Merlin" dell'Università e del Politecnico di Bari, I-70126 Bari, Italy

[13]Istituto Nazionale di Fisica Nucleare, Sezione di Bari, 70126 Bari, Italy

[14]Laboratoire Leprince-Ringuet, École polytechnique, CNRS/IN2P3, Palaiseau, France

[15]Institut de Ciencies de l'Espai (IEEC-CSIC), Campus UAB, 08193 Barcelona, Spain

[16]INAF-Istituto di Astrofisica Spaziale e Fisica Cosmica, I-20133 Milano, Italy

[17]Agenzia Spaziale Italiana (ASI) Science Data Center, I-00044 Frascati (Roma), Italy

[18]NASA Goddard Space Flight Center, Greenbelt, MD 20771, USA

[19]Center for Research and Exploration in Space Science and Technology (CRESST) and NASA Goddard Space Flight Center, Greenbelt, MD 20771, USA

[20]Department of Physics and Center for Space Sciences and Technology, University of Maryland Baltimore County, Baltimore, MD 21250, USA

[21]George Mason University, Fairfax, VA 22030, USA

[22]Laboratoire de Physique Théorique et Astroparticules, Université Montpellier 2, CNRS/IN2P3, Montpellier, France

[23]Department of Physics, Stockholm University, AlbaNova, SE-106 91 Stockholm, Sweden

[24]The Oskar Klein Centre for Cosmoparticle Physics, AlbaNova, SE-106 91 Stockholm, Sweden

[25]Royal Swedish Academy of Sciences Research Fellow, funded by a grant from the K. A. Wallenberg Foundation

[26]CNRS/IN2P3, Centre d'Études Nucléaires Bordeaux Gradignan, UMR 5797, Gradignan, 33175, France

[27]Université de Bordeaux, Centre d'Études Nucléaires Bordeaux Gradignan, UMR 5797, Gradignan, 33175, France

[28]Dipartimento di Fisica, Università di Udine and Istituto Nazionale di Fisica Nucleare, Sezione di Trieste, Gruppo Collegato di Udine, I-33100 Udine, Italy

[29]Osservatorio Astronomico di Trieste, Istituto Nazionale di Astrofisica, I-34143 Trieste, Italy

[30]Max-Planck-Institut für Radioastronomie, Auf dem Hügel 69, 53121 Bonn, Germany

[31]Department of Physical Sciences, Hiroshima University, Higashi-Hiroshima, Hiroshima 739-8526, Japan

[32]INAF Istituto di Radioastronomia, 40129 Bologna, Italy

[33]Center for Space Plasma and Aeronomic Research (CSPAR), University of Alabama in Huntsville, Huntsville, AL 35899, USA

[34]Department of Physics, Center for Cosmology and Astro-Particle Physics, The Ohio State University, Columbus, OH 43210, USA

[35]Department of Physics and Department of Astronomy, University of Maryland, College Park, MD 20742, USA

[36]Research Institute for Science and Engineering, Waseda University, 3-4-1, Okubo, Shinjuku, Tokyo, 169-8555 Japan

[37]Centre d'Étude Spatiale des Rayonnements, CNRS/UPS, BP 44346, F-30128 Toulouse Cedex 4, France

[38]Istituto Nazionale di Fisica Nucleare, Sezione di Roma "Tor Vergata", I-00133 Roma, Italy

[39]Department of Physics and Astronomy, University of Denver, Denver, CO 80208, USA

[40]Hiroshima Astrophysical Science Center, Hiroshima University, Higashi-Hiroshima, Hiroshima 739-8526, Japan

[41]Institute of Space and Astronautical Science, JAXA, 3-1-1 Yoshinodai, Sagamihara, Kanagawa 229-8510, Japan

[42]Max-Planck Institut für extraterrestrische Physik, 85748 Garching, Germany

[43]Institut für Astro- und Teilchenphysik and Institut für Theoretische Physik, Leopold-Franzens-Universität Innsbruck, A-6020 Innsbruck, Austria

[44]Kavli Institute for Cosmological Physics, University of Chicago, Chicago, IL 60637, USA; lreyes@kicp.uchicago.edu

[45]Santa Cruz Institute for Particle Physics, Department of Physics and Department of Astronomy and Astrophysics, University of California at Santa Cruz, Santa Cruz, CA 95064, USA

[46]Department of Physics, University of Washington, Seattle, WA 98195-1560, USA

[47]Space Sciences Division, NASA Ames Research Center, Moffett Field, CA 94035-1000, USA

[48]Department of Chemistry and Physics, Purdue University Calumet, Hammond, IN 46323-2094, USA

[49]Partially supported by the International Doctorate on Astroparticle Physics (IDAPP) program

[50]Institució Catalana de Recerca i Estudis Avançats (ICREA), Barcelona, Spain

[51]Consorzio Interuniversitario per la Fisica Spaziale (CIFS), I-10133 Torino, Italy

[52]INTEGRAL Science Data Centre, CH-1290 Versoix, Switzerland

[53]Dipartimento di Fisica, Università di Roma "Tor Vergata", I-00133 Roma, Italy

[54]Department of Physics, Royal Institute of Technology (KTH), AlbaNova, SE-106 91 Stockholm, Sweden

[55]School of Pure and Applied Natural Sciences, University of Kalmar, SE-391 82 Kalmar, Sweden

[56]Fred Lawrence Whipple Observatory, Harvard-Smithsonian Center for Astrophysics, Amado, AZ 85645, USA

[57]Department of Physics and Astronomy, Barnard College, Columbia University, NY 10027, USA

[58]Department of Physics and Astronomy, University of California, Los Angeles, CA 90095, USA

[59]Santa Cruz Institute for Particle Physics and Department of Physics, University of California, Santa Cruz, CA 95064, USA

[60]Department of Physics, Washington University, St. Louis, MO 63130, USA

[61]Astrophysical Institute, Department of Physics and Astronomy, Ohio University, Athens, OH 45701

[62]Department of Physics and Astronomy and the Bartol Research Institute, University of Delaware, Newark, DE 19716, USA

[63]School of Physics and Astronomy, University of Leeds, Leeds, LS2 9JT, UK

[64]Argonne National Laboratory, 9700 S. Cass Avenue, Argonne, IL 60439, USA

[65]School of Physics, University College Dublin, Belfield, Dublin 4, Ireland

[66]School of Physics, National University of Ireland Galway, University Road, Galway, Ireland

[67]Physics Department, California Polytechnic State University, San Luis Obispo, CA 94307, USA

[68]Astronomy Department, Adler Planetarium and Astronomy Museum, Chicago, IL 60605, USA

[69]Department of Physics, Purdue University, West Lafayette, IN 47907, USA

[70]European Space Astronomy Centre (INSA-ESAC), European Space Agency (ESA), Satellite Tracking Station, P.O.Box - Apdo 50727, 28080 Villafranca del Castillo, Madrid, Spain

[71]Department of Astronomy and Astrophysics, 525 Davey Lab, Pennsylvania State University, University Park, PA 16802, USA

[72]Department of Physics and Astronomy, University of Utah, Salt Lake City, UT 84112, USA

[73]Physics Department, McGill University, Montreal, QC H3A 2T8, Canada

[74]Enrico Fermi Institute, University of Chicago, Chicago, IL 60637, USA

[75]Department of Physics and Astronomy, Iowa State University, Ames, IA 50011, USA

[76]Department of Physics and Astronomy, University of Iowa, Van Allen Hall, Iowa City, IA 52242, USA

[77]Department of Physics and Astronomy, DePauw University, Greencastle, IN 46135-0037, USA

[78]Department of Physics, Pittsburg State University, 1701 South Broadway, Pittsburg, KS 66762, USA

[79]Department of Life and Physical Sciences, Galway-Mayo Institute of Technology, Dublin Road, Galway, Ireland

[80]Instituto de Astronomia y Fisica del Espacio, Casilla de Correo 67 - Sucursal 28, (C1428ZAA) Ciudad Autnoma de Buenos Aires, Argentina

[81]Department of Applied Physics and Instrumentation, Cork Institute of Technology, Bishopstown, Cork, Ireland

[82]Columbia Astrophysics Laboratory, Columbia University, New York, NY 10027, USA

[83]INAF, Osservatorio Astronomico di Torino, Italy

[84]Harvard-Smithsonian Center for Astrophysics, MA, USA

[85]Astronomical Institute, St.-Petersburg State University, Russia

[86]Pulkovo Observatory, Russia

[87]Isaac Newton Institute of Chile, St.-Petersburg Branch, Russia

[88]Abastumani Observatory, Mt. Kanobili, 0301 Abastumani, Georgia

[89]Department of Astronomy, University of Michigan, MI, USA

[90]Metsähovi Radio Observatory, Helsinki University of Technology TKK, Finland

[91]Institute of Astronomy, National Central University, Taiwan

[92]Tuorla Observatory, Department of Physics and Astronomy, University of Turku, Finland

[93]Instituto de Astrofísica de Andalucía, CSIC, Spain

[94]Max-Planck-Institut für Radioastronomie, Germany

[95]Institute of Astronomy, Bulgarian Academy of Sciences, Bulgaria

[96]Circolo Astrofili Talmassons, Italy

[97]Instituto de Astronomía, Universidad Nacional Autónoma de México, Apdo. Postal 70-265, CP 04510, México DF, México

[98]INAF, Osservatorio Astrofisico di Catania, Italy

[99]Astrophysical Institute, Department of Physics and Astronomy, Ohio University, OH, USA

[100]Osservatorio Astronomico della Regione Autonoma Valle d'Aosta, Italy

[101]Armenzano Astronomical Observatory, Italy

[102]INAF, Osservatorio Astronomico di Roma, Italy

[103]INAF, Osservatorio Astronomico di Collurania Teramo, Italy

[104]Agrupació Astronòmica de Sabadell, Spain

[105]ZAH, Landessternwarte Heidelberg, Königstuhl, 69117, Heidelberg, Germany

[106]Instituto de Astronomía, Universidad Nacional Autónoma deMéxico, Apdo. Postal 877, CP 22800, Ensenada, B.C., México

[107]Institute for Astrophysical Research, Boston University, MA, USA

[108]DLR, Institute of Planetary Research,Rutherfordstr. 2, 12489 Berlin, Germany

[109]INAOE, Apdo. Postal 51 & 216, 72000 Tonantzintla,Puebla, México

[110]Finnish Centre for Astronomy with ESO (FINCA), University of Turku,Väisäläntie 20, FI-21500 Piikkiö, Finland

[111]Department of Physics, University of Colorado Denver, CO, USA

[112]INAF - Osservatorio Astronomico di Brera, via E. Bianchi 46, 23807, Merate, Italy

[113]Department of Astrophysical Sciences, Princeton University, Princeton, NJ 08544, USA

[114]Department of Astronomy, University of California, Berkeley, CA 94720-3411, USA

[115]Max-Planck-Institut für Radioastronomie, Auf dem Hügel 69, 53121 Bonn, Germany

[116]Department of Astronomy and Astrophysics, University of California, 1156 High Street, Santa Cruz, CA 95064, USA

[117]Landessternwarte, Universität Heidelberg,Königstuhl 12, D 69117 Heidelberg, Germany

[118]UCO/Lick Observatory, University of California, 1156 High Street, Santa Cruz, CA 95064, USA

[119]Institut de Radio Astronomie Millimétrique, Avenida Divina Pastora 7, Local20, 18012 Granada, Spain

ABSTRACT

The BL Lacertae object 3C 66A was detected in a flaring state by the *Fermi* Large Area Telescope (LAT) and VERITAS in 2008 October. In addition to these gamma-ray observations, F-GAMMA, GASP-WEBT, PAIRITEL, MDM, ATOM, *Swift*, and *Chandra* provided radio to X-ray coverage. The available light curves show variability and, in particular, correlated flares are observed in the optical and *Fermi*-LAT gamma-ray band. The resulting spectral energy distribution can be well fit using standard leptonic models with and without an external radiation field for inverse-Compton scattering. It is found, however, that only the model with an external radiation field can accommodate the intra-night variability observed at optical wavelengths.

Subject headings: BL Lacertae objects: individual (3C 66A) — galaxies: active — gamma rays: observations

1.   Introduction

The radio source 3C 66 (Bennett 1962) was shown by Mackay (1971) and Northover (1973) to actually consist of two unrelated radio sources separated by $0.11°$: a compact source (3C 66A) and a resolved galaxy (3C 66B). 3C 66A was subsequently identified as a quasi-stellar object by Wills & Wills (1974), and as a BL Lacertae object by Smith et al. (1976) based on its optical spectrum. 3C 66A is now a well-known blazar which, like other active galactic nuclei (AGN), is thought to be powered by accretion of material onto a supermassive black hole located in the central region of the host galaxy (Urry & Padovani 1995). Some AGN present strong relativistic outflows in the form of jets, where particles are believed to be accelerated to ultra-relativistic energies and gamma rays are subsequently produced. Blazars are the particular subset of AGN with jets aligned to the observer's line of sight. Indeed, the jet of 3C 66A has been imaged using very long baseline interferometry (VLBI) (Taylor et al. 1996; Jorstad et al. 2001; Marscher et al. 2002; Britzen et al. 2007) and superluminal motion has been inferred (Jorstad et al. 2001; Britzen et al. 2008). This is indicative of the relativistic Lorentz factor of the jet and its small angle with respect to the line of sight.

BL Lacs are known for having very weak (if any) detectable emission lines, which makes determination of their redshift quite difficult. The redshift of 3C 66A was reported as $z = 0.444$ by Miller et al. (1978) and also (although tentatively) by Kinney et al. (1991). Each measurement

[120] Now at DESY, Platanenallee 6, 15738 Zeuthen, Germany

[121] Now at Institut für Physik und Astronomie, Universität Potsdam, 14476 Potsdam-Golm,Germany; DESY, Platanenallee 6, 15738 Zeuthen, Germany

[122] Now at Los Alamos National Laboratory, MS H803, Los Alamos, NM 87545

however, is based on the measurement of a single line and is not reliable (Bramel et al. 2005). Recent efforts (described in Section 2.5) to provide further constraints have proven unsuccessful.

Similar to other blazars, the spectral energy distribution (SED) of 3C 66A has two pronounced peaks, which suggests that at least two different physical emission processes are at work (e.g., Joshi & Böttcher 2007). The first peak, extending from radio to soft X-ray frequencies, is likely due to synchrotron emission from high-energy electrons, while different emission models have been proposed to explain the second peak, which extends up to gamma-ray energies. Given the location of its synchrotron peak ($\lesssim 10^{15}$ Hz), 3C 66A is further sub-classified as an intermediate synchrotron peaked blazar (ISP) (Abdo et al. 2010c).

The models that have been proposed to explain gamma-ray emission in blazars can be roughly categorized into leptonic or hadronic, depending on whether the accelerated particles responsible for the gamma-ray emission are primarily electrons and positrons (hereafter "electrons") or protons. In leptonic models, high-energy electrons produce gamma rays via inverse Compton scattering of low-energy photons. In synchrotron self-Compton (SSC) models, the same population of electrons responsible for the observed gamma rays generates the low-energy photon field through synchrotron emission. In external Compton (EC) models the low-energy photons originate outside the emission volume of the gamma rays. Possible sources of target photons include: accretion-disk photons radiated directly into the jet (Dermer & Schlickeiser 1993), accretion-disk photons scattered by emission-line clouds or dust into the jet (Sikora et al. 1994), synchrotron radiation re-scattered back into the jet by broad-line emission clouds (Ghisellini & Madau 1996), jet emission from an outer slow jet sheet (Ghisellini et al. 2005), or emission from faster or slower portions of the jet (Georganopoulos & Kazanas 2004). In hadronic models, gamma rays are produced by high-energy protons, either via proton synchrotron radiation (Mücke et al. 2003), or via secondary emission from photo-pion and photo-pair-production reactions (see Böttcher (2007) and references therein for a review of blazar gamma-ray emission processes).

One of the main obstacles in the broadband study of gamma-ray blazars is the lack of simultaneity, or at least contemporaneousness, of the data at the various wavelengths. At high energies the situation is made even more difficult due to the lack of objects that can be detected by MeV/GeV and TeV observatories on comparable time scales. Indeed, until recently the knowledge of blazars at gamma-ray energies had been obtained from observations performed in two disjoint energy regimes: i) the high energy (HE) range (20 MeV$< E < 10$ GeV), studied in the 1990s by EGRET (Thompson et al. 1993), and ii) the very-high-energy (VHE) regime (E > 100 GeV) observed by ground-based instruments (Weekes 2000). Only[1] Markarian 421 was detected by both EGRET and the first imaging atmospheric Cherenkov telescopes (Kerrick et al. 1995). Furthermore, blazars detected by EGRET at MeV/GeV energies are predominantly flat-spectrum radio quasars (FSRQs), while TeV blazars are, to date, predominantly BL Lacs. It is important to understand these observational differences since they are likely related to the physics of the AGN

---

[1]Markarian 501 was marginally detected by EGRET only during a few months in 1996 (Kataoka et al. 1999).

(Cavaliere & D'Elia 2002), or to the evolution of blazars over cosmic time (Böttcher & Dermer 2002).

The current generation of gamma-ray instruments (AGILE, *Fermi*, H.E.S.S., MAGIC and VERITAS) is closing the gap between the two energy regimes due to improved instrument sensitivities, leading us towards a deeper and more complete characterization of blazars as high-energy sources and as a population (Abdo et al. 2009b). An example of the successful synergy of space-borne and ground-based observatories is provided by the joint observations of 3C 66A by *Fermi* and VERITAS during its strong flare of 2008 October. The flare was originally reported by VERITAS (Swordy 2008; Acciari et al. 2009), and soon after, contemporaneous variability was also detected at optical to infrared wavelengths (Larionov et al. 2008), and in the *Fermi*-LAT energy band (Tosti 2008). Follow-up observations were obtained at radio, optical and X-ray wavelengths in order to measure the flux and spectral variability of the source across the electromagnetic spectrum and to obtain a quasi-simultaneous SED. This paper reports the results of this campaign, including the broadband spectrum and a model interpretation of this constraining SED.

2. Observations and Data Analysis

2.1. VERITAS

The Very Energetic Radiation Imaging Telescope Array System (VERITAS) is an array of four 12m diameter imaging atmospheric Cherenkov telescopes (IACTs) in southern Arizona, U.S.A. (Acciari et al. 2008b). 3C 66A was observed with VERITAS for 14 hours from 2007 September through 2008 January and for 46 hours between 2008 September and 2008 November. These observations (hereafter 2007-2008 data) add up to $\sim$32.8 hours of live time after data quality selection. The data were analyzed following the procedure described in Acciari et al. (2008b).

As reported in Acciari et al. (2009), the average spectrum measured by VERITAS is very soft, yielding a photon index Γ of 4.1 $\pm 0.4_{stat} \pm 0.6_{sys}$ when fitted to a power law $dN/dE \propto E^{-\Gamma}$. The average integral flux above 200 GeV measured by VERITAS is $(1.3 \pm 0.1) \times 10^{-11}$ cm^{-2} s^{-1}, which corresponds to 6% of the Crab Nebula's flux above this threshold. In addition, a strong flare with night-by-night VHE-flux variability was detected in October 2008. For this analysis the VERITAS spectrum is calculated for the short time interval October 8 – 10, 2008 (MJD 54747-54749; hereafter *flare* period), and for a longer period corresponding to the *dark run*[2] where most of the VHE emission from 3C 66A was detected (MJD 54734 - 54749). It should be noted that the *flare* and *dark run* intervals overlap and are therefore not independent. Table 1 lists the relevant information from each data set.

---

[2]Imaging atmospheric Cherenkov telescopes (IACTs) like VERITAS do not operate on nights with bright moonlight. The series of nights between consecutive bright-moonlight periods is usually referred as a *dark run*.

As shown in Figure 1, the *flare* and *dark run* spectra are very soft, yielding nearly identical photon indices of $4.1 \pm 0.6_{stat} \pm 0.6_{sys}$, entirely consistent with that derived from the full 2007-2008 data set. The integral flux above 200 GeV for the *flare* period is $(2.5 \pm 0.4) \times 10^{-11}$ cm^{-2} s^{-1}, while the average flux for the *dark run* period is $(1.4 \pm 0.2) \times 10^{-11}$ cm^{-2} s^{-1}. The extragalactic background light (EBL) de-absorbed spectral points for the *dark run* calculated using the optical depth values of (Franceschini et al. 2008) and assuming a nominal redshift of $z = 0.444$, are also shown in Figure 1. These points are well fit by a power law function with $\Gamma = 1.9 \pm 0.5$.

2.2. *Fermi*-LAT

The Large Area Telescope (LAT) on board the *Fermi* Gamma-ray Space Telescope is a pair-conversion detector sensitive to gamma rays with energies between 20 MeV and several hundred GeV (Atwood et al. 2009). Since launch the instrument has operated almost exclusively in sky survey mode, covering the whole sky every 3 hours. The overall coverage of the sky is fairly uniform, with exposure variations of $\leq 15\%$ around the mean value. The LAT data are analyzed using ScienceTools v9r15p5 and instrument response functions P6V3 (available via the *Fermi* science support center[3]). Only photons in the *diffuse* event class are selected for this analysis because of their reduced charged-particle background contamination and very good angular reconstruction. A zenith angle $<105°$ cut in instrument coordinates is used to avoid gamma rays from the Earth limb. The diffuse emission from the Galaxy is modeled using a spatial model (`gll_iem_v02.fit`) which was refined with *Fermi*-LAT data taken during the first year of operation. The extragalactic diffuse and residual instrumental backgrounds are modeled as an isotropic component and are included in the fit[4]. The data are analyzed with an unbinned maximum likelihood technique (Mattox et al. 1996) using the likelihood analysis software developed by the LAT team.

Although 3C 66A was detected by EGRET as source 3EG J0222+4253 (Hartman et al. 1999), detailed spatial and timing analyses by Kuiper et al. (2000) showed that this EGRET source actually consists of the superposition of 3C 66A and the nearby millisecond pulsar PSR J0218+4232 which is $0.96°$ distant from the blazar. This interpretation of the EGRET data is verified by *Fermi*-LAT, whose improved angular resolution permits the clear separation of the two sources as shown in Figure 2. Furthermore, the known pulsar period is detected with high confidence in the *Fermi*-LAT data (Abdo et al. 2009a). More importantly for this analysis, the clear separation between the pulsar and the blazar enables studies of each source independently in the maximum likelihood analysis, and thus permits an accurate determination of the spectrum and localization of each source, with negligible contamination.

Figure 2 also shows the localization of the *Fermi* and VERITAS sources with respect to blazar

---

[3]http://fermi.gsfc.nasa.gov/ssc/data/analysis/scitools/overview.html

[4]http://fermi.gsfc.nasa.gov/ssc/data/access/lat/BackgroundModels.html

3C 66A and radio galaxy 3C 66B (see caption in Figure 2 for details). It is clear from the map that the *Fermi*-LAT and VERITAS localizations are consistent and that the gamma-ray emission is confidently associated with the blazar and not with the radio galaxy. Some small contribution in the *Fermi*-LAT data from radio galaxy 3C 66B as suggested by Aliu et al. (2009) and Tavecchio & Ghisellini (2009) cannot be excluded given the large spill-over of low-energy photons from 3C 66A at the location of 3C 66B. This is due to the long tails of the *Fermi*-LAT point-spread-function at low energies as described in Atwood et al. (2009). Nevertheless, considering only photons with energy $E > 1$ GeV, the upper limit (95% confidence level) for a source at the location of 3C 66B is 2.9 x 10^{-8}cm^{-2}s^{-1} for the *dark run* period (with a test statistic[5] $TS = 1.3$). For the 11 months of data corresponding to the first *Fermi*-LAT catalog (Abdo et al. 2010a) the upper limit is 4.9 x 10^{-9}cm^{-2}s^{-1} ($TS = 5.8$).

As in the analysis of the VERITAS observations, the *Fermi*-LAT spectrum is calculated for the *flare* and for the *dark run* periods. The *Fermi flare* period flux $F(E > 100\text{MeV}) = (5.0 \pm 1.4_{\text{stat}} \pm 0.3_{\text{sys}})$ x 10^{-7}cm^{-2}s^{-1} is consistent within errors with the *dark run* flux of $(3.9 \pm 0.5_{\text{stat}} \pm 0.3_{\text{sys}})$ x 10^{-7}cm^{-2}s^{-1}. In both cases the *Fermi*-LAT spectrum is quite hard and can be described by a power law with a photon index Γ of $1.8 \pm 0.1_{\text{stat}} \pm 0.1_{\text{sys}}$ and $1.9 \pm 0.1_{\text{stat}} \pm 0.1_{\text{sys}}$ in the *flare* period and *dark run* intervals, respectively. Both spectra are shown in the high-energy SED in Figure 1.

2.3. *Chandra*

3C 66A was observed by the *Chandra* observatory on October 6, 2008 for a total of 37.6 ksec with the Advanced CCD Imaging Spectrometer (ACIS), covering the energy band between 0.3 and 10 keV. The source was observed in the continuous clocking (CC) mode to avoid pile-up effects. Standard analysis tools (CIAO 4.1) and calibration files (CALDB v3.5.0) provided by the Chandra X-ray center[6] are used.

The time-averaged spectrum is obtained and re-binned to ensure that each spectral channel contains at least 25 background-subtracted counts. This condition allows the use of the χ^2 quality-of-fit estimator to find the best fit model. XSPEC v12.4 (Arnaud 1996) is used for the spectral analysis and fitting procedure.

Two spectral models have been used to fit the data: single power law and broken power law. Each model includes galactic H I column density ($N_{H,\text{Gal}} = 8.99 \times 10^{20}$ cm^{-2}) according to Dickey & Lockman (1990), where the photoelectric absorption is set with the XSPEC model *phabs*[7].

---

[5]The test statistic value (TS) quantifies the probability of having a point source at the location specified. It is roughly the square of the significance value: a TS of 25 corresponds to a signal of approximately 5 standard deviations (Abdo et al. 2010a).

[6]http://cxc.harvard.edu/ciao/

[7]http://heasarc.gsfc.nasa.gov/docs/software/lheasoft/xanadu/xspec/manual/XSmodelPhabs.html

Interval	Live Time [hr]	N_{On}	N_{Off}	Alpha	Excess	Significance [σ]
flare	6.0	1531	7072	0.121	678.3	18.0
dark run	21.2	3888	20452	0.125	1331.5	22.2
2007-2008	28.1	7257	31201	0.175	1791	21.1

Table 1: Results from VERITAS observations of 3C 66A. Live time corresponds to the effective exposure time after accounting for data quality selection. N_{On} (N_{Off}) corresponds to the number of on(off)-source events passing background-rejection cuts. Alpha is the normalization of off-source events and the excess is equal to $N_{\mathrm{On}} - \alpha N_{\mathrm{Off}}$. The significance is expressed in number of standard deviations and is calculated according to equation (17) of Li & Ma (1983). See Acciari et al. (2009) for a complete description of the VERITAS analysis.
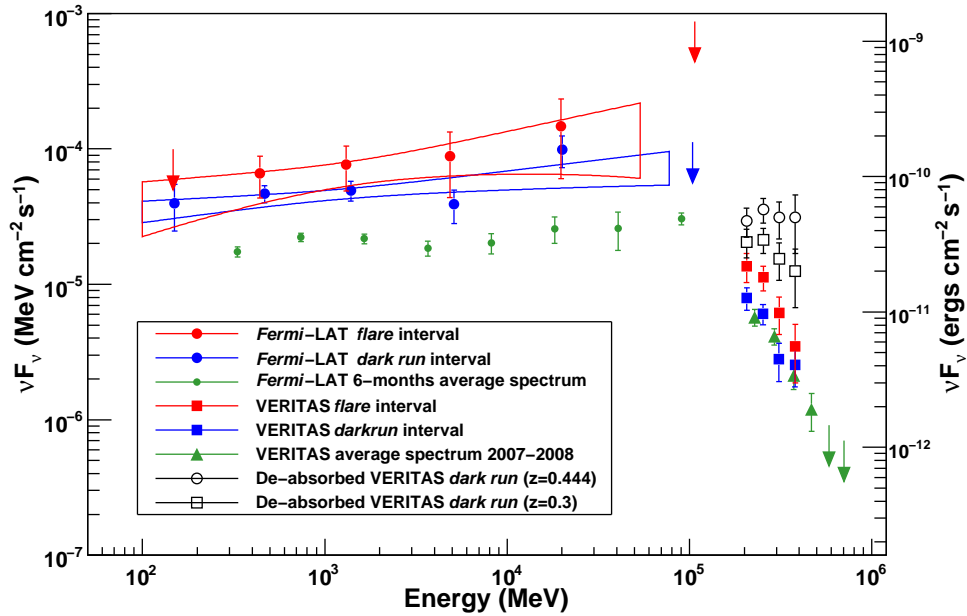

Fig. 1.— Gamma-ray SED of 3C 66A including *Fermi*-LAT and VERITAS data for the *flare* (red symbols) and *dark run* (blue symbols) intervals. The *Fermi*-LAT spectra is also shown here as "butterfly" contours (solid lines) describing the statistical error on the spectrum (Abdo et al. 2009b). The previously reported *Fermi*-LAT 6-month-average spectrum (Abdo et al. 2010b) is also shown here (green circles) and is lower than the spectrum obtained during the campaign. The average 2007–2008 VERITAS spectrum originally reported in Acciari et al. (2009) is displayed with green triangles. In all cases the upper limits are calculated at 95% confidence level. The de-absorbed *dark run* spectra obtained using the optical depth values of Franceschini et al. (2008) are also shown as open circles and open squares for redshifts of 0.444 and 0.3, respectively.
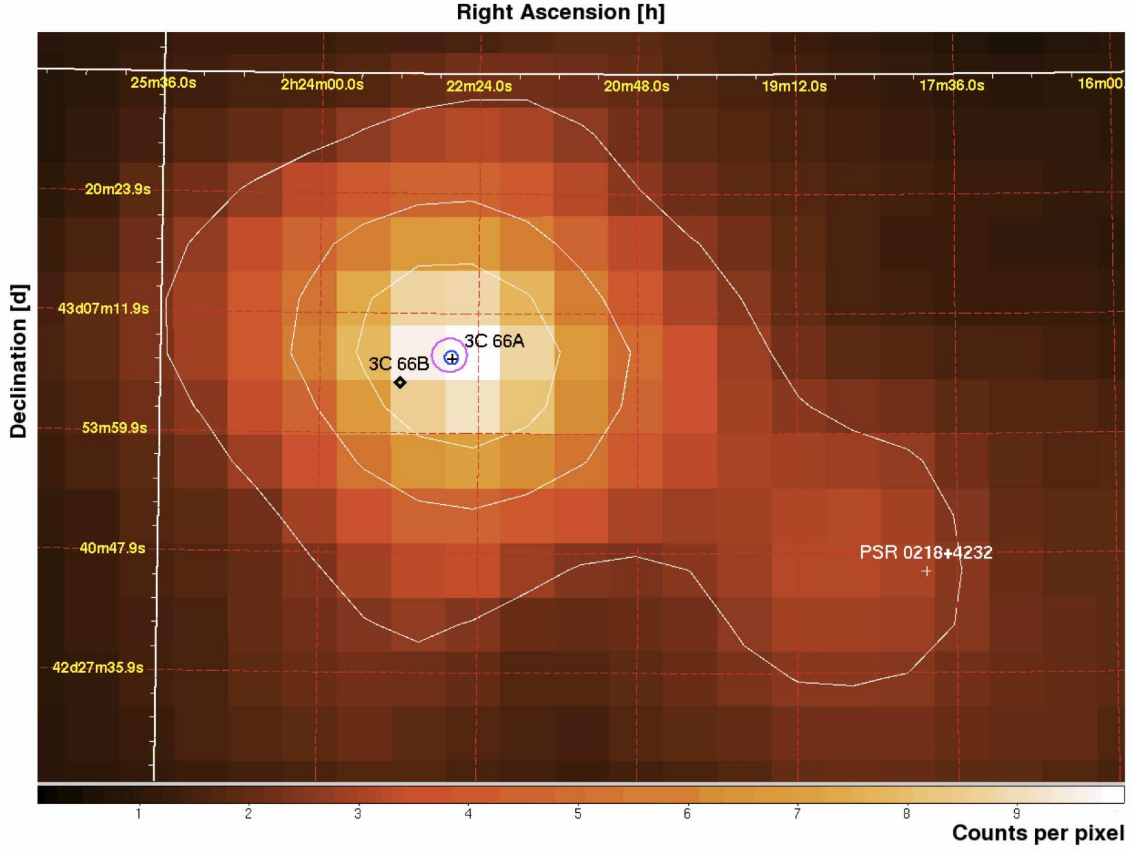
Fig. 2.— Smoothed count map of the 3C 66A region as seen by *Fermi*-LAT between September 1, 2008 and December 31, 2008 with E>100 MeV. The color bar has units of counts per pixel and the pixel dimensions are $0.1° \times 0.1°$. The contour levels have been smoothed and correspond to 2.8, 5.2, and 7.6 counts per pixel. The locations of 3C 66A and 3C 66B (a radio galaxy that is $0.11°$ away) are shown as a cross and as a diamond, respectively. The location of millisecond pulsar PSR 0218+4232 is also indicated with a white cross. The magenta circle represents the VERITAS localization of the VHE source (RA; DEC) = $(2^h \quad 22^m \quad 41.6^s \pm 1.7^s_{stat} \pm 6.0^s_{sys}$; $43° \quad 02' \quad 35.5"$ $\pm 21"_{stat} \pm 1'30"_{sys}$) as reported in Acciari et al. (2009). The blue interior circle represents the 95% error radius of the *Fermi*-LAT localization (RA; DEC) = $(02^h \quad 22^m \quad 40.3^s \pm 4.5^s$; $43° \quad 02' \quad 18.6"$ $\pm 42.1"$) as reported in the *Fermi*-LAT first source catalog (Abdo et al. 2010a). All positions are based on the J2000 epoch.

An additional local H I column density was also tried but in both cases the spectra was consistent with pure galactic density. Consequently, the column density has been fixed to the galactic value in each model and the obtained results are presented in Table 2. An F-test was performed to demonstrate that the spectral fit improves significantly when using the extra degrees of freedom of the broken power law model. Table 2 also contains the results of the F-test.

2.4. *Swift* XRT and UVOT

Following the VERITAS detection of VHE emission from 3C 66A, Target of Opportunity (ToO) observations of 3C 66A with *Swift* were obtained for a total duration of ∼10 ksec. The *Swift* satellite observatory comprises an UV-Optical telescope (UVOT), an X-ray telescope (XRT) and a Burst Alert Telescope (Gehrels et al. 2004). Data reduction and calibration of the XRT data are performed with *HEASoft* v6.5 standard tools. All XRT data presented here are taken in Photon Counting (PC) mode with negligible pile-up effects. The X-ray spectrum of each observation is fit with an absorbed power law using a fixed Galactic column density from Dickey & Lockman (1990), which gives good χ^2 values for all observations. The measured photon spectral index ranges between 2.5 and 2.9 with a typical statistical uncertainty of 0.1.

UVOT obtained data through each of six color filters, V, B and U together with filters defining three ultraviolet passbands, $UVW1$, $UVM2$ and $UVW2$ with central wavelengths of 260 nm, 220 nm and 193 nm respectively. The data are calibrated using standard techniques (Poole et al. 2008) and corrected for Galactic extinction by interpolating the absorption values from Schlegel et al. (1998) ($E_{B-V} = 0.083$ mag) with the galactic spectral extinction model of Fitzpatrick (1999).

2.5. Optical to Infrared Observations

The R magnitude of the host galaxy of 3C 66A is ∼19 in the optical band (Wurtz et al. 1996). Its contribution is negligible compared to the typical AGN magnitude of $R \lesssim 15$, therefore host-galaxy correction is not necessary.

GASP-WEBT: 3C 66A is continuously monitored by telescopes affiliated to the GLAST-AGILE support program of the Whole Earth Blazar Telescope (GASP-WEBT; see Villata et al. (2008, 2009)). These observations provide a long-term light curve of this object with complete sampling as shown in Figure 3. During the time interval in consideration (MJD 54700 - 54840), several observatories (Abastumani, Crimean, L'Ampolla, Lulin, New Mexico Skies, Roque de los Muchachos (KVA), Rozhen, Sabadell, San Pedro Martir, St. Petersburg, Talmassons, Teide (BRT), and Tuorla) contributed photometric observations in the R band. Data in the J, H and K band were taken at the Campo Imperatore observatory. A list of the observatories and their location is available in Table 3.

Single Power Law Model		
Γ	Flux [10^{-12} ergs cm^{-2} s^{-1}]	$\chi^2/d.o.f.$
2.99±0.03	3.47±0.06	1.21 (232.6/193)
Broken Power Law Model					
Γ_1	Γ_2	Flux [10^{-12} ergs cm^{-2} s^{-1}]	Break [keV]	$\chi^2/d.o.f.$	F-test Prob.
$3.08^{+0.3}_{-0.5}$	$2.24^{+0.23}_{0.37}$	$3.58^{+0.07}_{-0.08}$	$3.3^{+0.5}_{-0.3}$	0.97 (185.2/191)	3.47×10^{-10}

Table 2: Best-fit model parameters for a fit performed to the *Chandra* data in the $1-7$ keV energy range. The galactic $N_{H,Gal}$ value is fixed to 8.99×10^{20} cm^{-2}, the value of the galactic H I column density according to Dickey & Lockman (1990). Errors indicate the 90% confidence level.

Observatory	Location	Web page
Radio Observatories		
Crimean Radio Obs.	Ukraine	www.crao.crimea.ua
Effelsberg	Germany	www.mpifr.de/english/radiotelescope
IRAM	Spain	www.iram-institute.org/EN/30-meter-telescope.php
Medicina	Italy	www.med.ira.inaf.it
Metsähovi	Finland	www.metsahovi.fi/en
Noto	Italy	www.noto.ira.inaf.it
UMRAO	Michigan, USA	www.astro.lsa.umich.edu/obs/radiotel
Infrared Observatories		
Campo Imperatore	Italy	www.oa-teramo.inaf.it
PAIRITEL	Arizona, USA	www.pairitel.org
Optical Observatories		
Abastumani	Georgia	www.genao.org
Armenzano	Italy	www.webalice.it/dcarosati
ATOM	Namibia	http://www.lsw.uni-heidelberg.de/projects/hess/ATOM/
Crimean Astr. Obs.	Ukraine	www.crao.crimea.ua
Kitt Peak (MDM)	Arizona, USA	www.astro.lsa.umich.edu/obs/mdm
L'Ampolla	Spain	
Lulin	Taiwan	www.lulin.ncu.edu.tw/english
New Mexico Skies Obs.	New Mexico, USA	www.nmskies.com
Roque (KVA)	Canary Islands, Spain	www.otri.iac.es/eno/nt.htm
Rozhen	Bulgaria	www.astro.bas.bg/rozhen.html
Sabadell	Spain	www.astrosabadell.org/html/es/observatoriosab.htm
San Pedro Mártir	México	www.astrossp.unam.mx/indexspm.html
St. Petersburg	Russia	www.gao.spb.ru
Talmassons	Italy	www.castfvg.it
Teide (BRT)	Canary Islands, Spain	www.telescope.org
Torino	Italy	www.to.astro.it
Tuorla	Finland	www.astro.utu.fi
Valle d' Aosta	Italy	www.oavda.it/english/osservatorio
Gamma-ray Observatories		
VERITAS	Arizona, USA	veritas.sao.arizona.edu

Table 3: List of ground-based observatories that participated in this campaign.

MDM: Following the discovery of VHE emission, 3C 66A was observed with the 1.3m telescope of the MDM Observatory during the nights of Oct. 6 - 10, 2008. A total of 290 science frames in U, B, V, and R bands (58 each) were taken throughout the entire visibility period (approx. 4:30 – 10:00 UT) during each night. The light curves, which cover the time around the flare, are presented in Figure 4.

ATOM: Optical observations for this campaign in the R band were also obtained with the 0.8 m optical telescope ATOM in Namibia which monitors this source periodically. Twenty photometric observations are available starting on MJD 54740 and are shown in Figures 3 and 4.

PAIRITEL: Near-infrared observations in the J, H and K_s were obtained following the VHE flare with the 1.3m Peters Automated Infrared Imaging Telescope (PAIRITEL; see Bloom et al. (2006)) located at the Fred Lawrence Whipple Observatory. The resulting light curves using differential photometry with four nearby calibration stars are shown in Figure 4.

Keck: The optical spectrum of 3C 66A was measured with the LRIS spectrometer (Oke et al. 1995) on the Keck I telescope on the night of 2009 September 17 under good conditions. The instrument configuration resulted in a full-width-half-maximum of ~ 250 km s^{-1} over the wavelength range 3200–5500Å (blue side) and ~ 200 km s^{-1} over the range 6350–9000Å (red side). A series of exposures totaling 110 seconds (blue) and 50 seconds (red) were obtained, yielding a signal-to-noise (S/N) per resolution element of ~ 250 and 230 for the blue and red cameras respectively. The data were reduced with the LowRedux[8] pipeline and calibrated using a spectrophotometric star observed on the same night. Inspection of the 3C 66A spectrum reveals no spectral features aside from those imposed by Earth's atmosphere and the Milky Way (Ca H+K). Therefore, these new data do not offer any insight on the redshift of 3C 66A and in particular are unable to confirm the previously reported value of $z = 0.444$ (Miller et al. 1978).

2.6. Radio Observations

Radio observations are available thanks to the F-GAMMA (Fermi-Gamma-ray Space Telescope AGN Multi-frequency Monitoring Alliance) program, which is dedicated to monthly monitoring of selected *Fermi*-LAT blazars (Fuhrmann et al. 2007; Angelakis et al. 2008). Radio flux density measurements were conducted with the 100-m Effelsberg radio telescope at 4.85, 8.35, 10.45, and 14.60 GHz on 2008 October 16. These data are supplemented with an additional measurement at 86 GHz conducted with the IRAM 30-m telescope (Pico Veleta, Spain), on 2008 October 8. The data were reduced using standard procedures described in Fuhrmann et al. (2008). Additional radio observations taken between October 5 and October 15, 2008 (contemporaneous to the *flare* period) are provided by the Medicina, Metsähovi, Noto, and UMRAO observatories, all of which are members of the GASP-WEBT consortium.

---

[8]http://www.ucolick.org/∼xavier/LowRedux/index.html

3. Discussion

3.1. Light Curves

The resulting multiwavelength light curves from this campaign are shown in Figure 3 for those bands with long-term coverage and in Figure 4 for those observations that were obtained shortly before and after the gamma-ray flare. The VERITAS observations are combined to obtain nightly ($E > 200$ GeV) flux values since no evidence for intra-night variability is observed. The highest flux occurred on MJD 54749 and significant variability is observed during the whole interval (χ^2 probability less than 10^{-4} for a fit of a constant flux).

The temporal dependence of the *Fermi*-LAT photon index and integral flux above 100 MeV and 1 GeV are shown with time bins with width of 3 days in Figure 3. For those time intervals with no significant detection a 95%-confidence flux upper limit is calculated. The flux and photon index from the *Fermi*-LAT first source catalog (Abdo et al. 2010a) are shown as horizontal lines for comparison. These values correspond to the average flux and photon index measured during the first eleven months of *Fermi* operations, and thus span the time interval considered in the figures. It is evident from the plot that the VHE flare detected by VERITAS starting on MJD 54740 is coincident with a period of high flux in the *Fermi* energy band. The photon index during this time interval is consistent within errors with the average photon index $\Gamma = 1.95 \pm 0.03$ measured during the first 6 months of the *Fermi* mission (Abdo et al. 2010b).

Long-term and well-sampled light curves are available at optical and near-infrared wavelengths thanks to observations by GASP-WEBT, ATOM, MDM and PAIRITEL. Unfortunately, radio observations were too limited to obtain a light curve and no statement about variability in this band can be made. The best sampling is available for the R band, for which variations with a factor of $\gtrsim 2$ are observed in the long-term light curve. Furthermore, variability on time scales of less than a day is observed, as indicated in Figure 4, and as previously reported by Böttcher et al. (2009) following the WEBT (Whole Earth Blazar Telescope) campaign on 3C 66A in 2007-2008.

The increase in gamma-ray flux observed in the *Fermi* band seems contemporaneous with a period of increased flux in the optical, and to test this hypothesis, the discrete correlation function (DCF) is used (Edelson & Krolik 1988). Figure 5 shows the DCF of the F($E > 1$ GeV) gamma-ray band with respect to the R band with time-lag bins of 3, 5 and 7 days. The profile of the DCF is consistent for all time-lag bins, indicating that the result is independent of bin size. The DCF with time-lag bins of 3 days was fitted with a Gaussian function of the form $DCF(\tau) = C_{max} \times \exp{(\tau - \tau_0)^2/\sigma^2}$, where C_{max} is the peak value of the DCF, τ_0 is the delay timescale at which the DCF peaks, and σ parametrizes the Gaussian width of the DCF. The best fit function is plotted in Figure 5 and the best fit parameters are $C_{max} = 1.1 \pm 0.3$, $\tau_0 = (0.7 \pm 0.7)$ days and $\sigma = (3.3 \pm 0.7)$ days. An identical analysis was also performed between the F($E > 100$ MeV) and the R optical band with consistent results. This indicates a clear correlation between the *Fermi*-LAT and optical energy bands with a time lag that is consistent with zero and not greater than ~ 5
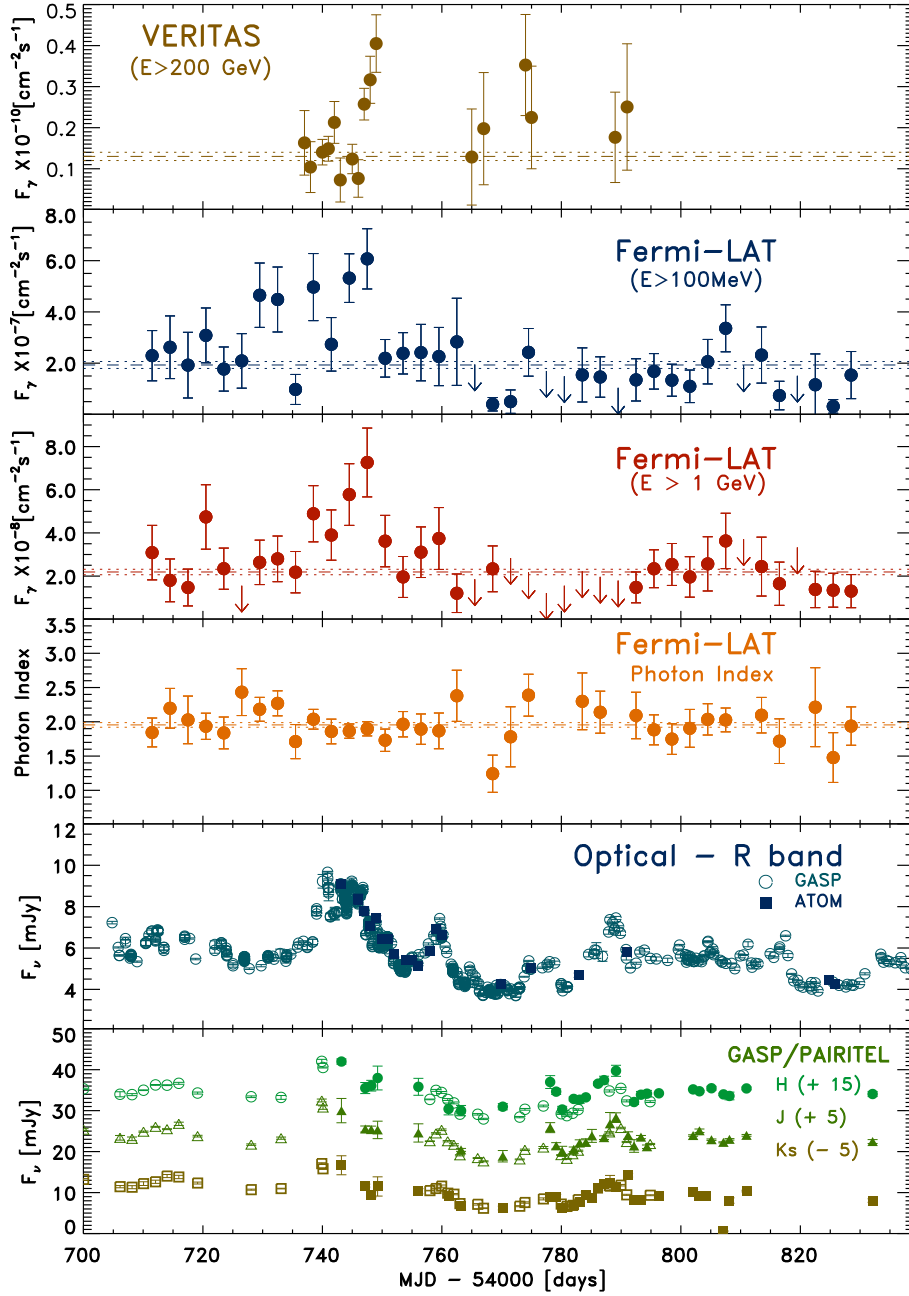
Fig. 3.— 3C 66A light curves covering 2008 Aug 22 to 2008 Dec 31 in order of increasing wavelength. The VERITAS observations are combined to obtain nightly flux values and the dashed and dotted lines represent the average flux measured from the 2007–2008 data and its standard deviation. The *Fermi*-LAT light curves contain time bins with a width of 3 days. The average flux and average photon index measured by Fermi-LAT during the first six months of science operations are shown as horizontal lines in the respective panels. In all cases the *Fermi*-LAT photon index is calculated over the 100 MeV to 200 GeV energy range. The long-term light curves at optical and infrared wavelengths are presented in the two bottom panels. In the bottom panel GASP-WEBT and PAIRITEL observations are represented by open and solid symbols, respectively.
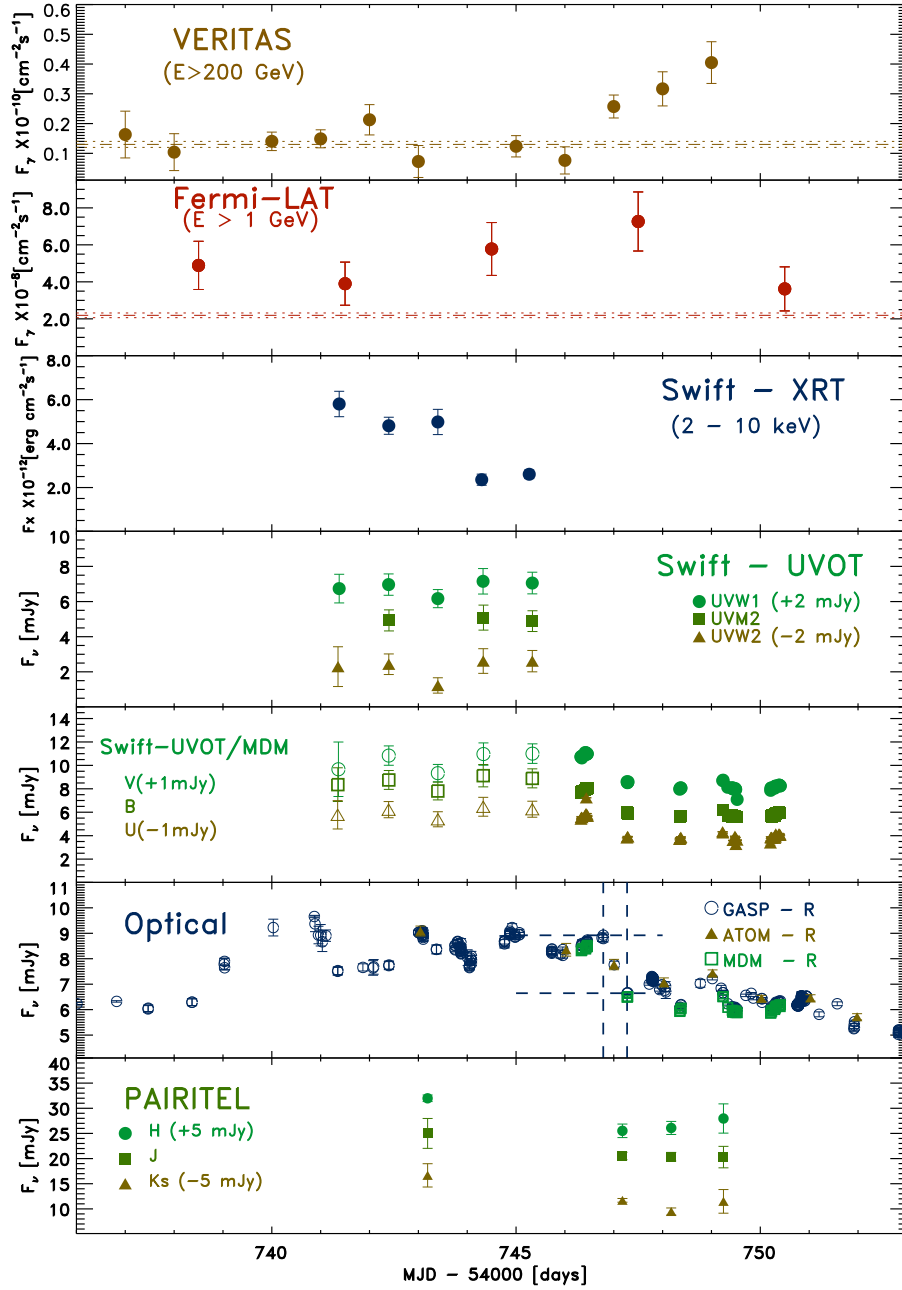
Fig. 4.— 3C 66A light curves covering the period centered on the gamma-ray flare (2008 Oct 1 - 10). The VERITAS and *Fermi*-LAT panels were already described in the caption of Figure 3. *Swift* Target-of-Opportunity (ToO) observations (panels 3-5 from the top) were obtained following the discovery of VHE emission by VERITAS (Swordy 2008). *Swift*-UVOT and MDM observations are represented by open and solid symbols, respectively. The optical light curve in panel 6 from the top displays intra-night variability. An example is identified in the plot, when a rapid decline of the optical flux by $\Delta F/\Delta t \sim -0.2$ mJy hr^{-1} is observed on MJD 54747.
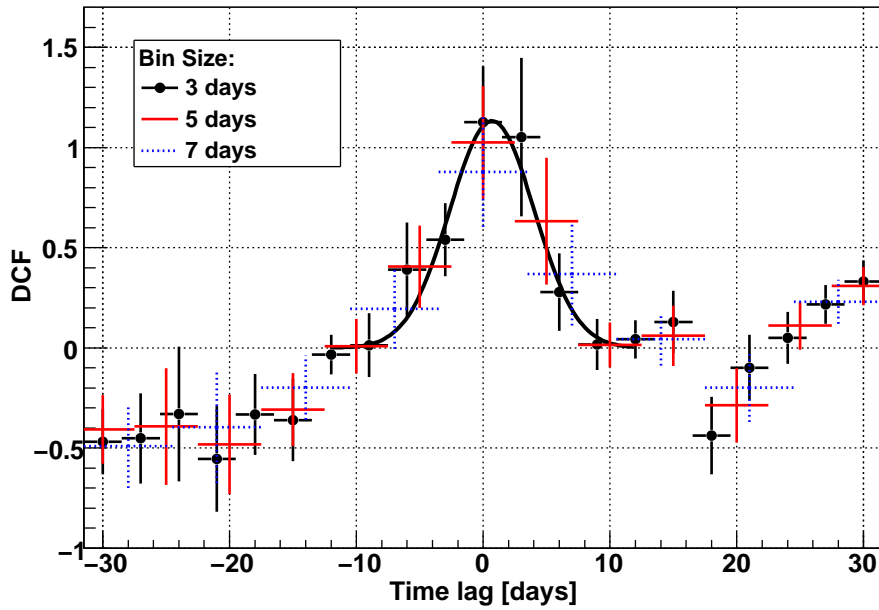
Fig. 5.— Discrete correlation function (DCF) of the F(E > 1 GeV) gamma-ray light curve with respect to the R band light curve. A positive time lag indicates that the gamma-ray band leads the optical band. Different symbols correspond to different bin sizes of time lag as indicated in the legend. The profile of the DCF is independent of bin size and is well described by a Gaussian function of the form $DCF(\tau) = C_{max} \times \exp{(\tau - \tau_0)^2/\sigma^2}$. The fit to the 3-day bin size distribution is shown in the plot as solid black line and the best-fit parameters are $C_{max} = 1.1 \pm 0.3$, $\tau_0 = (0.7 \pm 0.7)$ days and $\sigma = (3.3 \pm 0.7)$ days.

days. Despite the sparsity of the VERITAS light curve (due in part to the time periods when the source was not observable due to the full Moon) the DCF analysis was also performed to search for correlations with either the *Fermi*-LAT or optical data. Apart from the overall increase in flux, no significant correlations can be established. The onset of the E > 200 GeV flare seems delayed by about ∼5 days with respect to the optical-GeV flare but given the coverage gaps no firm conclusion can be drawn (e.g., the flare could have been already underway when the observations took place). No such lag is expected from the homogeneous model described in the next section but could arise in models with complex energy stratification and geometry in the emitting region.

3.2. SED and Modeling

The broadband SED derived from these observations is presented in Figure 6 and modeled using the code of Böttcher & Chiang (2002). In this model, a power-law distribution of ultrarelativistic electrons and/or pairs with lower and upper energy cutoffs at $\gamma_{\min}$ and $\gamma_{\max}$, respectively, and power-law index q is injected into a spherical region of co-moving radius R_B. The injection rate is normalized to an injection luminosity L_e, which is a free input parameter of the model. The model assumes a temporary equilibrium between particle injection, radiative cooling due to synchrotron and Compton losses, and particle escape on a time $t_{\rm esc} \equiv \eta_{\rm esc} R_B/c$, where $\eta_{\rm esc}$ is a scale parameter in the range ∼ 250-500. Both the internal synchrotron photon field (SSC) and external photon sources (EC) are considered as targets for Compton scattering. The emission region is moving with a bulk Lorentz factor Γ along the jet. To reduce the number of free parameters, we assume that the jet is oriented with respect to the line of sight at the superluminal angle so that the Doppler factor is equal to $D = (\Gamma [1 - \beta \cos\theta_{\rm obs}])^{-1} = \Gamma$, where $\theta_{\rm obs}$ is the angle of the jet with respect to the line of sight. Given the uncertainty in the redshift determination of 3C 66A, a range of plausible redshifts, namely $z = 0.1, 0.2, 0.3$, and the generally used catalog value $z = 0.444$ are considered for the modeling. All model fits include EBL absorption using the optical depth values from Franceschini et al. (2008).

Most VHE blazars known to date are high synchrotron peaked blazars (HSPs), whose SEDs can often be fit satisfactorily with pure SSC models. Since the transition from HSP to ISP is continuous, a pure SSC model was fit first to the radio through VHE gamma-ray SED. Independently of the model under consideration, the low-frequency part of the SED ($< 10^{20}$ Hz) is well fit with a synchrotron component, as shown in Figure 6. For clarity, only the high-frequency range is shown in Figures 7 and 8, where the different models are compared. As can be seen from the figure, a reasonable agreement with the overall SED can be achieved for any redshift in the explored range. The weighted sum of squared residuals has been calculated for the *Fermi*-LAT and VERITAS *flare* data (8 data points in total) in order to quantify the scatter of the points with respect to the model and is shown in Table 4. The best agreement is achieved when the source is located at $z \sim 0.2 - 0.3$. For lower redshifts, the model spectrum is systematically too hard, while at $z = 0.444$, the model spectrum is invariably too soft as a result of EBL absorption. It should be noted that the EBL
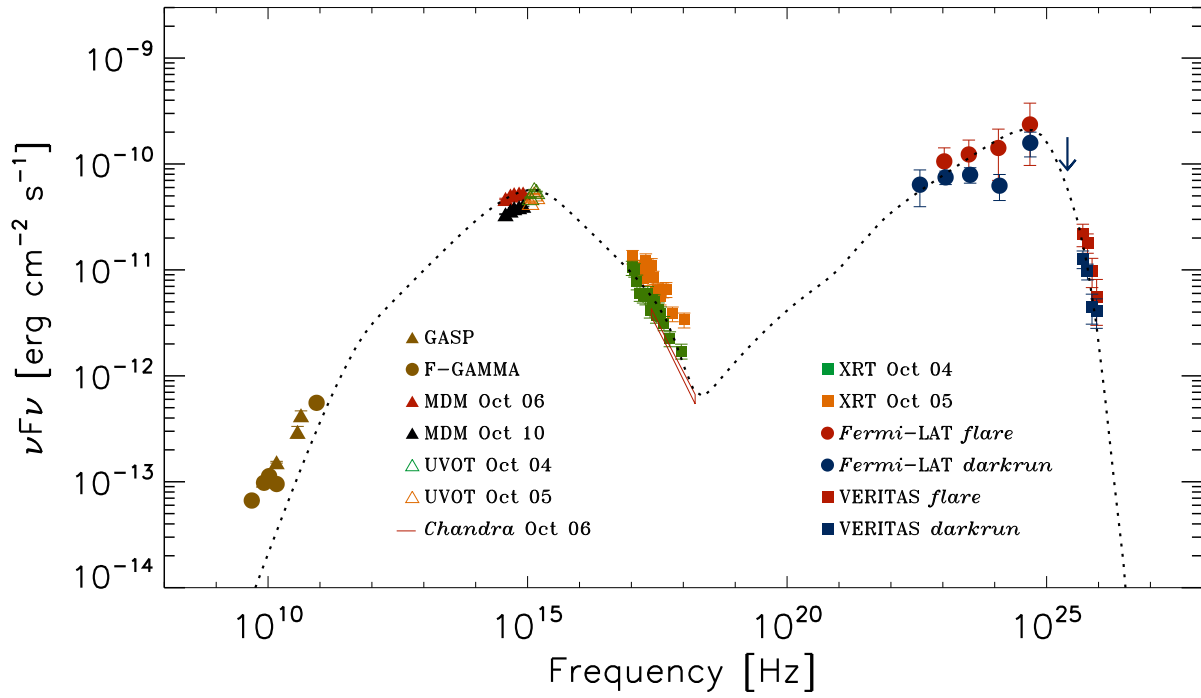
Fig. 6.— Broadband SED of 3C 66A during the October 2008 multiwavelength campaign. The observation that corresponds to each set of data points is indicated in the legend. As an example, the EBL-absorbed EC+SSC model for $z = 0.3$ is plotted here for reference. A description of the model is provided in the text.

model of Franceschini et al. (2008) predicts some of the lowest optical depth values in comparison to other models (Finke et al. 2010; Gilmore et al. 2009; Stecker et al. 2006). Thus, a model spectrum with redshift of 0.3 or above would be even harder to reconcile with the observations when using other EBL models.

A major problem of the SSC models with $z \gtrsim 0.1$ is that R_B is of the order of $\gtrsim 5 \times 10^{16}$ cm. This does not allow for variability time scales shorter than $\lesssim 1$ day, which seems to be in contrast with the optical variability observed on shorter time scales. A smaller R_B would require an increase in the electron energy density (with no change in the magnetic field in order to preserve the flux level of the synchrotron peak) and would lead to internal gamma-gamma absorption. This problem could be mitigated by choosing extremely high Doppler factors, $D \gtrsim 100$. However, these are significantly larger than the values inferred from VLBI observations of *Fermi*-LAT blazars (Savolainen et al. 2010)[9]. Moreover, all SSC models require very low magnetic fields, far below the value expected from equipartition ($\epsilon_B = L_B/L_e \sim 10^{-3} << 1$), where L_B is the Poynting flux derived from the magnetic energy density and L_e is the energy flux of the electrons propagating along the jet). Table 4 lists the parameters used for the SSC models displayed in Figure 7.

Subsequently, an external infrared radiation field with ad-hoc properties was included as a source of photons to be Compton scattered. For all SSC + EC models shown in Figure 8, the peak frequency of the external radiation field is set to $\nu_{\text{ext}} = 1.4 \times 10^{14}$ Hz, corresponding to near-IR. This adopted value is high enough to produce E $\gtrsim$ 100 GeV photons from inverse Compton scattering off the synchrotron electrons and at the same time is below the energy regime in which Klein-Nishina effects take place. Although the weighted sum of squared residuals for EC+SSC models are generally worse than for pure SSC models, reasonable agreement with the overall SED can still be achieved for redshifts $z \lesssim 0.3$. Furthermore, all SSC + EC models are consistent with a variability time scale of $\Delta t_{\text{var}} \sim 4$ hr. This is in better agreement with the observed variability at optical wavelengths than the pure SSC interpretation. Also, while the SSC + EC interpretation still requires sub-equipartition magnetic fields, the magnetic fields are significantly closer to equipartition than in the pure SSC case, with $L_B/L_e \sim 0.1$. The parameters of the SSC + EC models are listed in Table 5.

Models with and without EC component yield the best agreement with the SED if the source is located at a redshift $z \sim 0.2 - 0.3$. Of course, this depends on the EBL model used in the analysis. An EBL model that predicts higher attenuation than Franceschini et al. (2008) would lead to a lower redshift range and make it even more difficult to have agreement between the SED models and the data when the source is located at redshifts $z \gtrsim 0.4$. Finally, it is worth mentioning that the redshift range $z \sim 0.2 - 0.3$ is in agreement with previous estimates by Finke et al. (2008), who estimate the redshift of 3C 66A to be $z = 0.321$ based on the magnitude of the host galaxy, and by

---

[9]As a caveat, jet models with a decelerating flow (Georganopoulos & Kazanas 2003; Piner et al. 2008) or with inhomogeneous transverse structure (Ghisellini et al. 2005; Henri & Saugé 2006) can accommodate very high Doppler factors in the gamma-ray emitting region and still be consistent with the VLBI observations of the large scale jet.
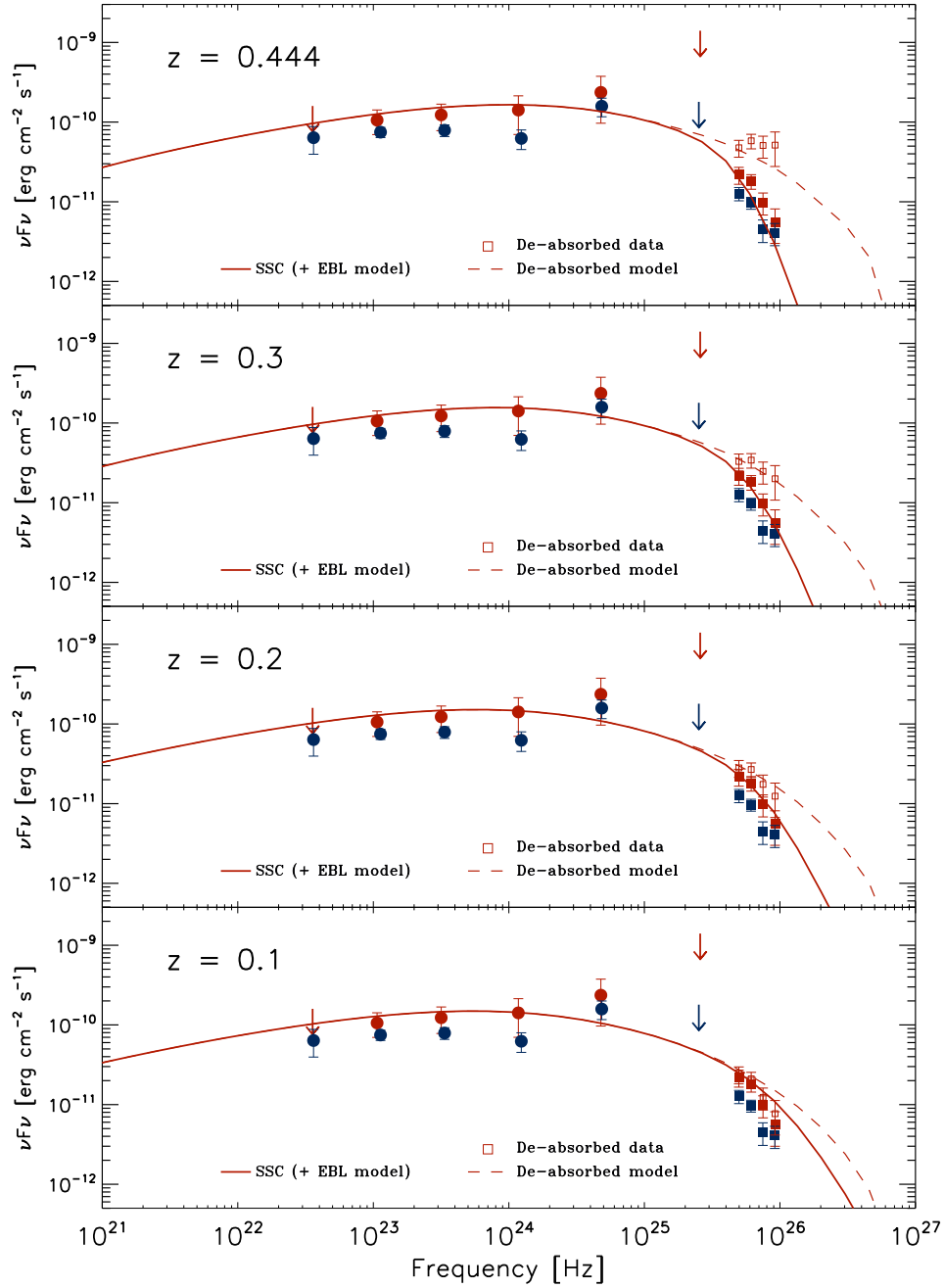
Fig. 7.— SSC models for redshifts z =0.444, 0.3, 0.2, and 0.1 from top to bottom. The *Fermi*-LAT and VERITAS data points follow the same convention used in Figures 1 and 6 to distinguish between *flare* (red) and *dark run* (blue) data points. In each panel the EBL-absorbed model is shown as a solid red line and the de-absorbed model as a red dashed line. De-absorbed VERITAS *flare* points are shown as open squares. In all cases the optical depth values from Franceschini et al. (2008) are used. The best agreement between the model and the data is achieved when the source is located at $z = 0.2 - 0.3$. For lower redshifts the model spectrum is systematically too hard, while at $z = 0.444$, the model spectrum is too soft.
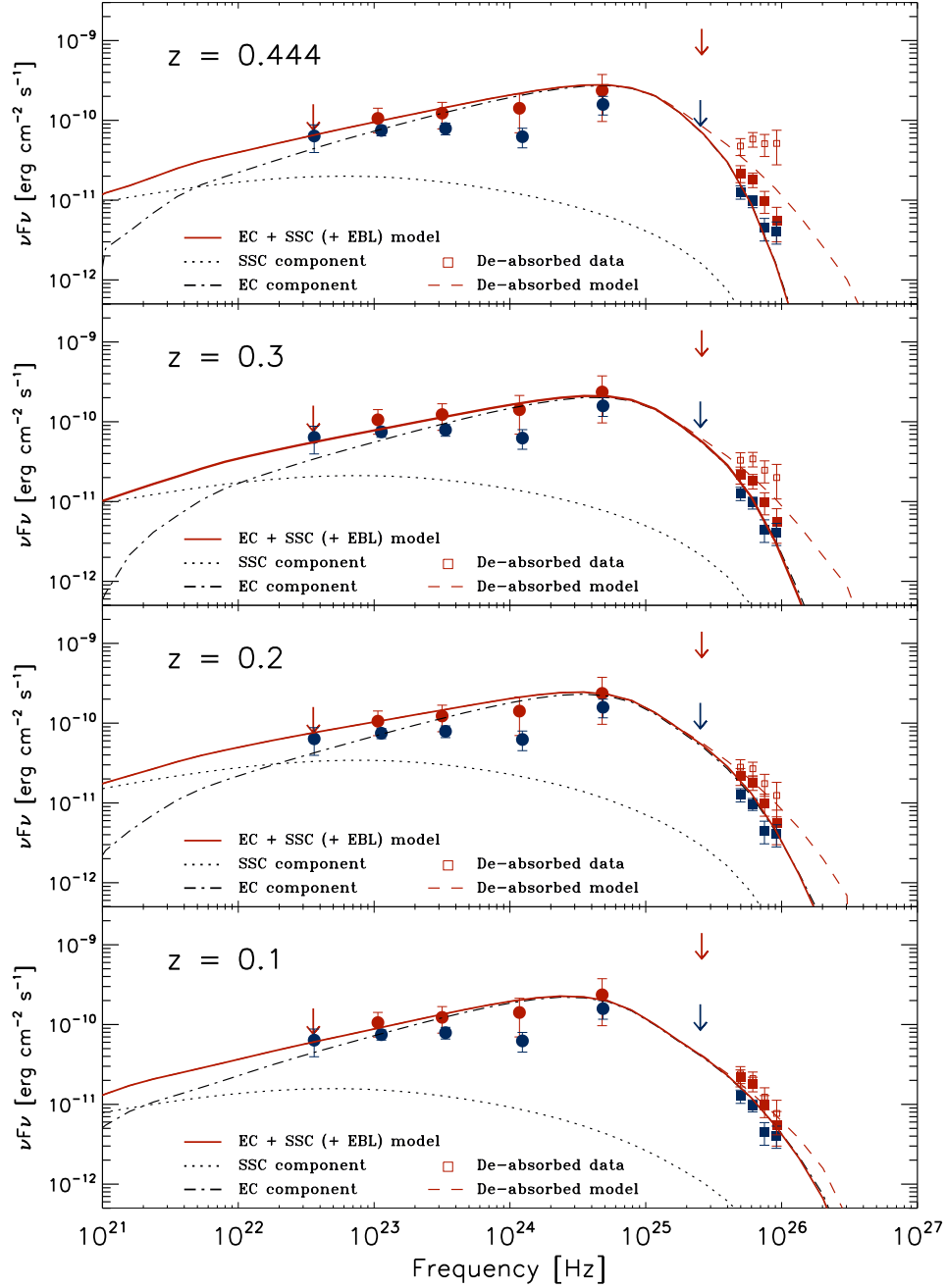
Fig. 8.— EC + SSC model for redshifts z =0.444, 0.3, 0.2, and 0.1 from top to bottom. The individual EBL-absorbed EC and SSC components are indicated as a dash-dotted and dotted lines, respectively. The sum is shown as solid red line (dashed when de-absorbed). The best agreement between the model and the data is achieved when the source is located at $z \sim 0.2$.

Prandini et al. (2010) who use an empirical relation between the previously reported *Fermi*-LAT and IACTs spectral slopes of blazars and their redshifts to estimate the redshift of 3C 66A to be below $z = 0.34 \pm 0.05$.

A detailed study of hadronic versus leptonic modeling of the October 2008 data will be published elsewhere, but it is worth mentioning that the synchrotron proton blazar (SPB) model has been used to adequately reproduce the quasi-simultaneous SED observed during the 2003-2004 multi-wavelength campaign (Reimer et al. 2008). On that occasion rapid intraday variations down to 2 hours time scale were observed, while during the 2008 campaign presented here these variations seem less rapid. Qualitatively, the longer time scale variations may be due to a lower Doppler beaming, at the same time that a strongly reprocessed proton synchrotron component dominates the high energy output of this source.

4. Summary

Multiwavelength observations of 3C 66A were carried out prompted by the gamma-ray outburst detected by the VERITAS and *Fermi* observatories in October 2008. This marks the first occasion that a gamma-ray flare is detected by GeV and TeV instruments in comparable time scales. The light curves obtained show strong variability at every observed wavelength and in particular, the flux increase observed by VERITAS and *Fermi* is coincident with an optical outburst. The clear correlation between the *Fermi*-LAT and R optical light curves permits one to go beyond the source association reported in the 1st *Fermi*-LAT source Catalog (Abdo et al. 2010a) and finally identify the gamma-ray source 1FGL J0222.6+4302 as blazar 3C 66A.

For the modeling of the overall SED a reasonable agreement can be achieved using both a pure SSC model and an SSC + EC model with an external near-infrared radiation field as an additional source for Compton scattering. However, the pure SSC model requires (a) a large emission region, which is inconsistent with the observed intra-night scale variability at optical wavelengths and (b) low magnetic fields, about a factor $\sim 10^{-3}$ below equipartition. In contrast, an SSC + EC interpretation allows for variability on time scales of a few hours, and for magnetic fields within about an order of magnitude of, though still below, equipartition. It is worth noting that the results presented here agree with the findings following the ($E > 200$ GeV) flare of blazar W Comae (also an ISP) in 2008 March (Acciari et al. 2008a). In both cases the high optical luminosity is expected to play a key role in providing the seed population for IC scattering.

Intermediate synchrotron peaked blazars like 3C 66A are well suited for simultaneous observations by *Fermi*-LAT and ground-based IACTs like VERITAS. Relative to the sensitivities of these instruments, ISPs are bright enough to allow for time-resolved spectral measurements in each band during flaring episodes. These types of observations coupled with extensive multi-wavelength coverage at lower energies will continue to provide key tests of blazar emission models.

Model parameter	$z = 0.1$	$z = 0.2$	$z = 0.3$	$z = 0.444$
Low-energy cutoff ($\gamma_{\min}$)	1.8×10^4	2.0×10^4	2.2×10^4	2.5×10^4
High-energy cutoff ($\gamma_{\max}$)	3.0×10^5	4.0×10^5	4.0×10^5	5.0×10^5
Injection index (q)	2.9	2.9	3.0	3.0
Injection luminosity (L_e) [10^{45} erg s^{-1}]	1.3	3.3	5.7	12.8
Co-moving magnetic field (B) [G]	0.03	0.02	0.02	0.01
Poynting flux (L_B) [10^{42} erg s^{-1}]	1.1	4.9	8.5	13.7
$\epsilon_B \equiv L_B/L_e$	0.9×10^{-3}	1.5×10^{-3}	1.5×10^{-3}	1.1×10^{-3}
Doppler factor (D)	30	30	40	50
Plasmoid radius (R_B) [10^{16} cm]	2.2	6.0	7.0	11
Variability time scale ($\delta t_{\mathrm{var}}^{\min}$) [hr]	7.4	22.1	21.1	29.4
Weighted sum of squared residuals to VERITAS *flare* data	7.1	0.9	0.7	6.2
Weighted sum of squared residuals to *Fermi*-LAT *flare* data	1.6	1.6	1.3	1.4
Total weighted sum of squared residuals	8.7	2.5	1.9	7.6

Table 4: Parameters used for the SSC models displayed in Figure 7. All SSC models require very low magnetic fields, far below the value expected from equipartition (i.e. $\epsilon_B << 1$). The weighted sum of squared residuals to the VERITAS and *Fermi*-LAT data and the total value for the combined data set are included at the bottom of the table. The best agreement between the model and the data is obtained when the source is at redshift $z = 0.2 - 0.3$.

Model parameter	$z = 0.1$	$z = 0.2$	$z = 0.3$	$z = 0.444$
Low-energy cutoff ($\gamma_{\min}$)	5.5×10^3	7.0×10^3	6.5×10^3	6.0×10^3
High-energy cutoff ($\gamma_{\max}$)	1.2×10^5	$1.51.2 \times 10^5$	$1.51.2 \times 10^5$	$1.51.2 \times 10^5$
Injection index (q)	3.0	3.0	3.0	3.0
Injection luminosity (L_e) [10^{44} erg s^{-1}]	1.1	4.2	6.0	10.4
Co-moving magnetic field (B) [G]	0.35	0.22	0.21	0.23
Poynting flux (L_B) [10^{43} erg s^{-1}]	1.0	2.4	6.0	11.2
$\epsilon_B \equiv L_B/L_e$	0.10	0.06	0.10	0.11
Doppler factor (D)	30	30	40	50
Plasmoid radius (R_B) [10^{16} cm]	0.5	1.2	1.5	1.5
Variability time scale ($\delta t_{\mathrm{var}}^{\min}$) [hr]	1.7	4.4	4.5	4.0
Ext. radiation energy density [10^{-6} erg cm^{-3}]	5.4	2.4	1.2	1.3
Weighted sum of squared residuals to VERITAS *flare* data	4.8	3.6	7.9	15.7
Weighted sum of squared residuals to *Fermi*-LAT *flare* data	1.0	1.2	0.8	1.5
Total weighted sum of squared residuals	5.8	4.8	8.7	17.2

Table 5: Parameters used for the EC+SSC model fits displayed in Figure 8. These model fits require magnetic fields closer to equipartition and allow for the intra-night variability observed in the optical data. The weighted sum of squared residuals to the VERITAS and *Fermi*-LAT data and the total value for the combined data set are included at the bottom of the table.

Acknowledgements

REFERENCES

Abdo, A. A., et al. 2009a, Science, 325, 848

Abdo, A. A., et al. 2009b, ApJ, 707, 1310

Abdo, A. A., et al. 2010a, ApJS, 188, 405

Abdo, A. A., et al. 2010b, ApJ, 710, 1271

Abdo, A. A., et al. 2010c, ApJ, 716, 30

Acciari, V. A., et al. 2008a, ApJ, 684, L73

Acciari, V. A., et al. 2008b, ApJ, 679, 1427

Acciari, V. A., et al. 2009, ApJ, 693, L104

Aliu, E., et al. 2009, ApJ, 692, L29

Angelakis, E., Fuhrmann, L., Marchili, N., Krichbaum, T. P., & Zensus, J. A. 2008, Memorie della Societa Astronomica Italiana, 79, 1042

Arnaud, K. A. 1996; in ASP Conf. Ser. 101: Astronomical Data Analysis Software and Systems (ADASS) V, 17.

Atwood, W. B., et al. 2009, ApJ, 697, 1071

Bennett, A. S. 1962, MmRAS, 68, 163

Böttcher, M., & Chiang, J. 2002, ApJ, 581, 127

Böttcher, M., & Dermer, C. D. 2002, ApJ, 564, 86

Böttcher, M. 2007, Ap&SS, 309, 95

Böttcher, M., et al. 2009, ApJ, 694, 174

Bloom, J. S., Starr, D. L., Blake, C. H., Skrutskie, M. F., & Falco, E. E. 2006, Astronomical Data Analysis Software and Systems XV, 351, 751

Bramel, D. A., et al. 2005, ApJ, 629, 108

Britzen, S., et al. 2007, A&A, 472, 763

Britzen, S., et al. 2008, A&A, 484, 119

Cavaliere, A., & D'Elia, V. 2002, ApJ, 571, 226

Dermer, C. D., & Schlickeiser, R. 1993, ApJ, 416, 458

Dickey, J. M., & Lockman, F. J. 1990, ARA&A, 28, 215

Edelson, R. A., & Krolik, J. H. 1988, ApJ, 333, 646

Finke, J. D., Shields, J. C., Böttcher, M., & Basu, S. 2008, A&A, 477, 513

Finke, J. D., Razzaque, S., & Dermer, C. D. 2010, ApJ, 712, 238

Fitzpatrick, E. L. 1999, PASP, 111, 63

Franceschini, A., Rodighiero, G., & Vaccari, M. 2008, A&A, 487, 837

Fuhrmann, L., et al. 2008, A&A, 490, 1019

Fuhrmann, L., Zensus, J. A., Krichbaum, T. P., Angelakis, E., & Readhead, A. C. S. 2007, The First GLAST Symposium, 921, 249

Gehrels, N., et al. 2004, ApJ, 611, 1005

Georganopoulos, M., & Kazanas, D. 2003, ApJ, 594, L27

Georganopoulos, M., & Kazanas, D. 2004, ApJ, 604, L81

Ghisellini, G., & Madau, P. 1996, MNRAS, 280, 67

Ghisellini, G., Tavecchio, F., & Chiaberge, M. 2005, A&A, 432, 401

Gilmore, R. C., Madau, P.,Primack, J. R., Somerville, R. S., & Haardt, F. 2009, MNRAS, 399, 1694

Hartman, R. C., et al. 1999, ApJS, 123, 79

Henri, G., & Saugé, L. 2006, ApJ, 640, 185

Jorstad, S. G., Marscher, A. P., Mattox, J. R., Wehrle, A. E., Bloom, S. D., & Yurchenko, A. V. 2001, ApJS, 134, 181

Joshi, M., & Böttcher, M. 2007, ApJ, 662, 884

Kataoka, J., et al. 1999, Astroparticle Physics, 11, 149

Kerrick, A. D., et al. 1995, ApJ, 452, 588

Kinney, A. L., Bohlin, R. C., Blades, J. C., & York, D. G. 1991, ApJS, 75, 645

Kuiper, L., Hermsen, W., Verbunt, F., Thompson, D. J., Stairs, I. H., Lyne, A. G., Strickman, M. S., & Cusumano, G. 2000, A&A, 359, 615

Larionov, V. M., et al. 2008, The Astronomer's Telegram, 1755, 1

Li, T.-P., & Ma, Y.-Q. 1983, ApJ, 272, 317

Mackay, C. D. 1971, MNRAS, 154, 209

Marscher, A. P., Jorstad, S. G., Mattox, J. R., & Wehrle, A. E. 2002, ApJ, 577, 85

Mattox, J. R., et al. 1996, ApJ, 461, 396

Miller, J. S., French, H. B., & Hawley, S. A. 1978, BL Lac Objects, 176

Mücke, A., Protheroe, R. J., Engel, R., Rachen, J. P., & Stanev, T. 2003, Astroparticle Physics, 18, 593

Northover, K. J. E. 1973, MNRAS, 165, 369

Oke, J. B., et al. 1995, PASP, 107, 375

Piner, B. G., Pant, N., & Edwards, P. G. 2008, ApJ, 678, 64

Prandini, E., Bonnoli, G., Maraschi, L., Mariotti, M., & Tavecchio, F. 2010, MNRAS, 405, L76

Poole, T. S., et al. 2008, MNRAS, 383, 627

Reimer, A., Joshi, M., & Böttcher, M. 2008, American Institute of Physics Conference Series, 1085, 502

Savolainen, T., Homan, D. C., Hovatta, T., Kadler, M., Kovalev, Y. Y., Lister, M. L., Ros, E., & Zensus, J. A. 2010, A&A, 512, A24

Schlegel, D. J., Finkbeiner, D. P., & Davis, M. 1998, ApJ, 500, 525

Sikora, M., Begelman, M. C., & Rees, M. J. 1994, ApJ, 421, 153

Smith, H. E., Smith, E. O., & Spinrad, H. 1976, PASP, 88, 621

Swordy, S. 2008, The Astronomer's Telegram, 1753, 1

Stecker, F. W., Malkan,M. A. & Scully, S. T. 2006, ApJ, 648, 774 and Erratum: ApJ, 658, 1392 (2007)

Tavecchio, F., & Ghisellini, G. 2009, MNRAS, 394, L131

Taylor, G. B., Vermeulen, R. C., Readhead, A. C. S., Pearson, T. J., Henstock, D. R., & Wilkinson, P. N. 1996, ApJS, 107, 37

Thompson, D. J., et al. 1993, ApJS, 86, 629

Tosti, G. 2008, The Astronomer's Telegram, 1759, 1

Urry, C. M., & Padovani, P. 1995, PASP, 107, 803

Villata, M., et al. 2008, A&A, 481, L79

Villata, M., et al. 2009, A&A, 504, L9

Weekes, T. C. 2000, American Institute of Physics Conference Series, 515, 3

Wills, B. J., & Wills, D. 1974, ApJ, 190, L97

Wurtz, R., Stocke, J. T., & Yee, H. K. C. 1996, ApJS, 103, 109